Implementation of the Prothrombin Time test in the *spinit*® point of care platform

Sofia Rodrigues Vaz
sofia.vaz@ist.utl.pt

Instituto Superior Técnico, Lisboa, Portugal

February 2016

Abstract

The prothrombin time blood assay is used by health specialists in the detection of cardiovascular anomalies, considered the leading cause of death in the world by the World Health Organisation.

Conventional clinical testing is time consuming, requires complex sample handling, and is prone to errors. However, recent technological advances have allowed the development of automatic, small, portable point of care (PoC) devices, that operate with small sample volumes, and can give results within minutes.

The present study proposes the integration of the prothrombin time assay in the *spinit*® centrifugal microfluidic platform, taking advantage of its photoelectric detection module, which allows to detect optical changes through paired emitter-detector diode ($PEDD$) based spectrophotometry.

The optical signal variation detected during fibrin formation was studied, and different relations were found between the *spinit*® output and the prothrombin time in international normalised ratio units (PT-INR) .

Several reagents were tested, the centrifugation protocol was optimised, and the optical system definitions were changed, in order to find the detection chamber as fast as possible.

Finally, the performance of different microfluidic mixing structures was evaluated experimentally, using plasma calibrators. Structure 24 from the 4th mixing layout tested allowed to obtain the best results, with coefficients of variation lower than 6% for all the calibrators, for all the time references considered.

Keywords: PT-INR, Prothrombin, PoC, Coagulation, PEDD

1. Introduction

In 2004 the *World Health Organization* (*WHO*) stated that cardiovascular diseases are the leading cause of death in the world. Also, according to the *International Self-Monitoring Association of Oral Anticoagulated Patients*, nearly four million people in Europe take anticoagulants and need to monitor their coagulation time daily [18, 5].

The human cardiovascular system is composed of a closed network of arteries, veins and capillaries in which blood is circulates. In case of rupture, a combination of processes occur in order to seal the rupture. Hemostasis is the result of mainly three distinct mechanisms intimately related that operate simultaneously: vascular constriction, platelet activity, and the production of stabilised fibrin through coagulation [1].

The coagulation model often mentioned is the coagulation cascade. It consists of a sequential series of steps in which the activation of one clotting factor (F) leads to the activation of another, finally leading to fibrin formation [16]. This model is outlined in a Y-shaped scheme with two distinct pathways called intrinsic and extrinsic, initiated by the activation of $FXII$ and $FVII$, respectively. They will then converge into a common pathway [1, 9]. A deficiency in the formation of any of the factors of both pathways may result in a prolongation of coagulation time as the cascade gets partially interrupted.

The prothrombin time (PT) test evaluates the functioning of the extrinsic and common pathways, by adding thromboplastin (or tissue factor) and calcium chloride to the sample. PT may vary substantially depending on the thromboplastin source, detection method and equipment used [11]. For these reasons, most laboratories express the results according to the International Normalized Ratio (INR), determined by eq.1. This ratio takes into account the reagent-device sensitivity through the International Sensitivity Index (ISI), usually between 1.0 and 2.0, that compares the system sensitivity to that of an international standard [11].

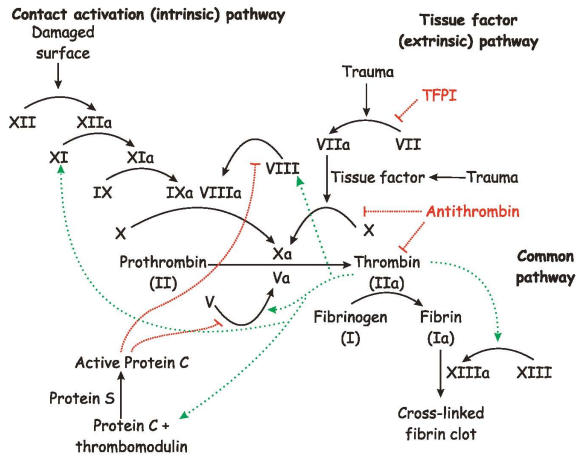

Figure 1: Simplified Coagulation cascade model, outlined in a Y-shaped scheme [2].

$$\mathrm{INR} = \left(\frac{\mathrm{PT_{Lab}}}{\text{Mean Normal PT}}\right)^{\mathrm{ISI}} \tag{1}$$

Recent technological advances have allowed the development of small portable devices called Point of Care (PoC), meant to perform blood testing near the patient. These devices usually require low power consumption, and use small blood sample and reagent volumes. The complexity of the tests performed can vary from simpler procedures to more complex ones, and the results are given within minutes. [17].

The main goal of this work is to develop the *PT-INR* test for *spinit*®, which is a microfluidic PoC platform developed by *biosurfit, SA*, using the photometric detection system it has incorporated.

2. Background

In PoC devices, both sample and reaction processing are made at a microlitre scale. Pressure, acoustic, electrokinetic and centrifuge fluid propulsion are the most common mechanisms for moving small fluid and suspended particle volumes at this scale[17].

Centrifugal pumps provide a large range of flow rates, and are relatively insensitive to physicochemical properties such as pH, ionic strength, or chemical composition. Valving can be done using capillary valves, in which capillary forces stop the fluid movement at a channel expansion until a rotationally induced pressure is sufficient to overcome them. Hydrophobic methods can also be used. In this case there is no real physical valve required. However, there is no simple way to stop vapours from spreading, which is inconvenient if liquids need to be stored for a long time inside the device [17].

The *spinit*® is a centrifugal microfluidic platform. The microfluidic elements are integrated in disposable discs, allowing reagents resuspension, blood separation, valving, mixing, metering, aliquoting and fluid delivery to the detection areas. The distribution of these elements is made from the centre of the disc to the outer radius. The sequence of actions performed relies on different force balances. Centrifugal and capillary forces allow the fluid to move away and towards the centre of rotation, respectively [4].

A fluid on a planar substrate rotating at a distance r from the centre at an angular velocity ω and a linear velocity v with a mass density ρ experiences a centrifugal force (eq.2), a Coriolis force (eq.3) and an Euler force (eq.4), all controlled by the variation of the angular velocity $\omega = \frac{v}{r}$ [4].

$$\vec{f}_{Centrif}(r) = \frac{F_{Centrif}(r)}{V} = \rho\frac{v^2}{r}\ \vec{e_r} = r\rho\omega^2\ \vec{e_r}, \tag{2}$$

$$\vec{f}_{Coriolis}(r) = -2\rho\omega v\ \vec{e_\theta}, \tag{3}$$

$$\vec{f}_{Euler}(r) = -\rho r\frac{d\omega}{dt}\ \vec{e_\theta}. \tag{4}$$

Capillary action occurs when liquid molecules adhesion to the walls is stronger than the cohesive forces between them. It can be quantified as a function of the pressure gradient ΔP that exists at the interface. Eq.5 describes the capillary force in a rectangular channel with width w and depth d. σ is the surface tension and θ is the contact angle between the fluid and the channel surface at the interface with air [12, 7]. Figure 2 shows the main forces that act on a disc spinning.

$$\vec{F}_{Cap} = \Delta P w d\ \vec{e_r} = -2\sigma\cos\theta\left(\frac{1}{w}+\frac{1}{d}\right) w d\ \vec{e_r} \tag{5}$$

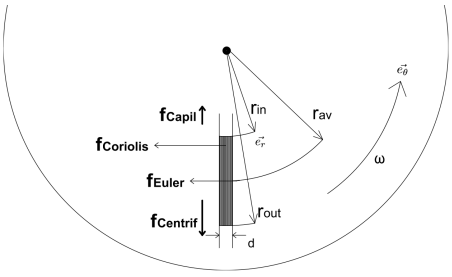

Figure 2: Geometry and forces on a disc spinning.

Resuspension and mixing are more challenging functions. The Reynolds Number R_e is a dimensionless quantity that is used to predict the flow behaviour of a fluid, depending on the linear dimensions l of the system, ρ, and also on the dynamic viscosity μ. The relation is expressed by eq.6:

$$R_e = \frac{l\rho v}{\mu} \tag{6}$$

In the microfluidic scale mixing is dominated by diffusion instead of convection, as the flow at this scale is laminar [17]. Diffusion is time-consuming and inefficient when the reaction occurs within seconds, as is the case with fibrin formation. In order to overcome this obstacle, several mixing mechanisms have been developed, both active and passive. Active methods are more efficient, however, they require an external energy supply and involve a complex fabrication process [13]. Passive methods, on the other hand, take advantage of physical and chemical phenomena such as gravity, capillary action, surface tension or osmosis. [10].

In 2014 Ju-Nan Kuo and Bo-Shiun Li proposed a simple centrifugal microfluidic platform for achieving rapid mixing of reagents in a seemingly low-cost way that consists on a serpentine structure [13]. This idea will be used further on.

2.1. PT Detection Systems Available

Measuring clotting times was, until recently, a procedure done only by highly trained lab staff. The main technique used consists in tilting back and forth a tube containing the blood sample and the reagent, until a visible fibrin clot is formed [13]. Nowadays, new automatic methods are being developed. They rely on different blood properties changes that occur during coagulation: viscosity, surface tension, electrical conductivity and optical density [5]. Some companies already provide *PoC* devices capable of performing the *PT-INR* test, however, most of them can only perform this one test, and use electrochemical and mechanical methods [3].

2.2. TIR and PEDD based Spectrophotometry

The *spinit*® photoelectric detection module relies on Total Internal Reflection (*TIR*) and also Paired Emitter-Detector Diode (*PEDD*) based Spectrophotometry.

The absorbance A of a sample, ratio between the incident intensity I_0 and the final intensity I of a light beam with a specific wavelength λ, can be related to the properties of the material through which the light is traveling, such as the initial concentration c of the substance, the molar extinction coefficient ϵ, and the optical path length l_{abs}, according to the Beer-Lambert Law (eq.7) [20]. This law does not specify what causes the light intensity decrease, which can occur due to absorption, scattering and/or reflection.

$$A = \log\left(\frac{I_0}{I}\right) = \ln(10)\ \epsilon(\lambda)\ c\ l_{abs} \qquad (7)$$

During fibrin formation an intensity I decrease is expected, because the sample becomes more viscous, leading to an increase in the refractive index of the medium and a consequent increase in light scattering [8].

Figure 3 represents the geometry of the photometry detection system inside the *spinit*®. A Light Emitting Diode (*LED*) emitts light perpendicularly to the disc surface, which is deflected 90° when it reaches a reflective structure via *TIR*. It then travels parallel to the disc surface, through the full length of the detection chamber, until it is reflected 90° again, and is finally detected by an *LED* operating in reverse mode. Similar geometries have already been used on other centrifugal microfluidic platforms [21, 20].

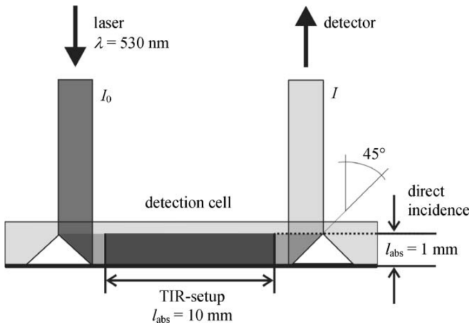

Figure 3: Optical light guidance by *TIR* at triangular prisms inclined 45° at the rear side of the surface. The values shown are the ones used in the experiment described in the article [20].

When light travels from a medium with refractive index n_1 to another medium with a higher n_2, according to the Snell's Law the critical angle α_c above which all the light is reflected is determined in eq.8. To ensure *TIR*, the angle of incidence has to exceed α_c [20, 21].

$$\alpha_c = \sin^{-1}\frac{n_1}{n_2}. \qquad (8)$$

Most polymers used in clinical diagnostics have a refractive index $n_2 \simeq 1.5$. If the light travels from air to these polymers $\alpha_c \simeq 41°$. Then, a structure like a triangular prism with a surface deviated 45° from the horizontal interface surface can deflect all the light emitted perpendicularly to the disc surface that reaches the prism [20, 21].

*LED*s are currently widely used in modern photoelectronics, because they are considered small, stable and robust low-powered light sources with a long lifetime expectancy. They cover a broad spectral range from ultraviolet (*UV*) to near infrared (*NIR*) wavelengths, at the same time having a narrow emission spectra [23, 19, 22].

The current-voltage characteristic of diodes in either forward or reverse mode is described by the Shockley Ideal Diode Equation (9), where i is the diode current, i_S is the saturation current, U is the voltage across the diode and $U_T = \frac{kT}{q}$ is the thermal voltage, which depends on the Boltzmann's constant k, the absolute p-n junction temperature

T and the elementary charge q [23, 6, 19].

$$i = i_S \left[e^{-\frac{U}{U_T}} - 1 \right] \simeq i = i_S e^{-\frac{U}{U_T}}, \quad (9)$$

The light intensity illuminating the detector-*LED*, I_L, is directly proportional to the current supplying the *LED*-emitter, i_C, so the exponential Shockley Equation 9 can be rewritten in the logarithmic form 10, where a and b are constants [23]:

$$U = a + b \log i_C = a + b \log I_L. \quad (10)$$

If the maximum light intensity $I_L = I_{max}$ is emitted directly into the detector, without travelling through a medium that can absorb or scatter light (the air can be considered such a medium), the detector will measure a corresponding maximum voltage U_{max}, assuming it is smaller than the saturation limit U_{sat} (eq.**??**). If light is emitted towards a sample (I_{sample}), the corresponding detection voltage is U_{sample}, and its value will vary depending on the characteristics of the sample (eq.11) [23].

$$U_{sample} = a + b \log I_{sample}. \quad (11)$$

Thus, the voltage difference measured by a *PEDD* device for a particular sample is directly proportional to the logarithm of the transmitted intensity (eq.12), and b represents the system sensitivity [23]:

$$\Delta U_{sample} = U_{max} - U_{sample} = b \log \left(\frac{I_{max}}{I_{sample}} \right) \quad (12)$$

In 2005 a Mitsubishi team developed a way of making very precise and accurate measurements of the photocurrent, using a simple threshold detector and a timer circuit. The idea is that a light detector-*LED* reverse biased and charged periodically with an initial voltage U_0 is discharged by the photocurrent i_{light} generated by the incoming light, until it reaches a lower threshold voltage U_t at a discharge instant t_d. The total discharge time t for the *LED* equivalent circuit can be described by eq.13, where Q is the accumulated charge and i_{dis} is a small current escape that is usually insignificant compared to i_{light}.$Q$is a constant, therefore, t is inversely proportional to the intensity of the detected light [15].

$$t = \frac{Q}{t_{dis} + i_{light}} \simeq \frac{Q}{i_{light}}. \quad (13)$$

3. Experimental Setup

Two *spinit*®s were used in the experiments, both fitted with an optical module. They have a stepper motor connected via *USB* to the motherboard for positioning the discs, and it also has a regular disc drive inside for spinning discs at high frequencies. Depending on the input commands given, the disc drive can perform several actions, including eject, inject, start and stop rotation, reaching a defined speed, rotate clockwise or counterclockwise, etc.

The electric board that controls the *LEDs* allows to detect saturation discharge times (DT) up to $65000 DT_0$ when measured in complete darkness, for the $605nm$ *LED*. $DT_0 = 0.512\mu s$ is the incorporated microprocessor internal clock unit, and will be the representation of the elementary discharge time unit from now on. Saturation discharge times may change depending on the emitter characteristics, such as its λ or maximum intensity.

The board also has another microchip with drivers installed in order to allow the *USB* to function as a Serial port. This enables communication between the board and the computer, allowing to send commands to each *LED* socket such as voltage settings to turn the *LEDs* ON and OFF, clear previous commands, setting the threshold voltage $U_t = 1.7V$, etc.

The *LED*s' setup used consists of an orange emitter *LED* with $\lambda = 605nm$ and half-viewing angle of 4°. The detector is an infrared photodiode *LED*.

3.1. Discs

Different disc constructions and layouts were used throughout the experiment. Changes in the layouts directly reflected the purpose of the study, whereas construction changes occurred mostly in order to keep up with parallel research being made at *biosurfit*.

The *spinit*® works with $1.2mm$ thick discs which can be composed of two $0.6mm$ bonded disc halves, or a single $1.2mm$ thick disc. An assembly process is required in both cases, and it varies depending on the materials used. In the first case, it is necessary to bond the two disc halves into one single piece, and in the second case it is necessary to seal the single $1.2mm$ disc.

In this work two different constructions were used. The first consisted of two *PC* half discs with a thickness of $0.6mm$, bonded with a hydrophilic film. One half disc has the chambers for both the reagent and the sample, as well as the microfluidic mixing structures. The other half disc has six detection chambers (with a $7.5mm$ optical path) and reflective structures shaped as triangular prisms, with walls making 45° from the horizontal surface, and a height of $200\mu m$. The second construction consisted of $1.2mm$ thick *PC* discs, bonded with a *PC* thin layer on top. These discs have more polished reflective prisms and 24 detection chambers, with a different shape from the previous six. The ones used have a $10mm$ optical path. This required the use of a different *spinit*® with the *LED*s setup in a different position. In this case the mixing structures and inlet chambers were milled directly on the prism discs.

The microfluidic layouts were designed using a standard *CAD* software, and the microfluidic mix-

ing structures are milled with a computer numeric control milling cutter (*CNC*) at *biosurfit*.

3.2. Reagents, calibrators and controls

Several reagents were tested: *Neoplastine® Cl Plus* from *Stago*, Thromboplastin from *Sigma Aldrich*, and Calcium Rabbit Brain Thromboplastin from *Diagen*. Calibrators from *Stago* and *Diagen* were used. The kit from *Stago* has 3 different levels, and the one from *Diagen* has 6 levels. Two controls from *Stago* were also used.

4. Results

The first tests were made manually, in order to understand if the clot formation was visible, and whether or not the coagulation time could be determined. There was no immediate visible change, unless the mixture was agitated vigorously, which on the other hand made it difficult to correctly assess coagulation time. Then, taking advantage of a spectrophotometer, a new series of tests were made, to see if the reaction could be detected optically. However, no variation was detected.

4.1. Paired emissor-detector device

Another system was used, represented in fig.4. It consists of a small rectangular prism with a rectangular cavity in the middle and two small holes in opposite sides, where *LEDs* can be put. The *LED*s were connected to an electric board similar to the one inside the *spinit®*. The results are presented in *DT* units.

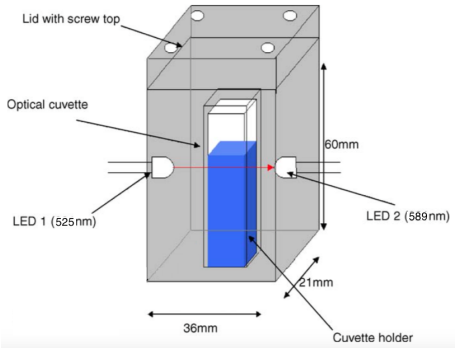

Figure 4: Setup used, similar to the one used in the experiment described in the article [14].

Several trials were made using the reagent and the controls from *Stago*, following the preparation recommendations strictly.Three different emission *LED*s ($\lambda = \{525, 589, 433\}$ nm) from *Roithner* were tested, with different emission intensities, until variations in signal were detected. The detection *LED* used in all trials had a $\lambda = 589$ nm. The biggest variation happened for the $\lambda = 525$ nm with an intensity of $\frac{40}{511} I_{max}$. This emitter was used in the next tests. Fig.5 shows an example obtained with 200 μL of a normal control from *Stago* added to 400 μL of *Neoplastine*.

All results obtained were similar in behaviour. They show an initial *DT* state plateau that corresponds to having only the control plasma/reagent in the cuvette, then, when the reagent/plasma is introduced, we can observe an abrupt variation followed by a second state plateau with a very small negative inclination. Finally, the *DT* starts raising until a third state plateau is formed.

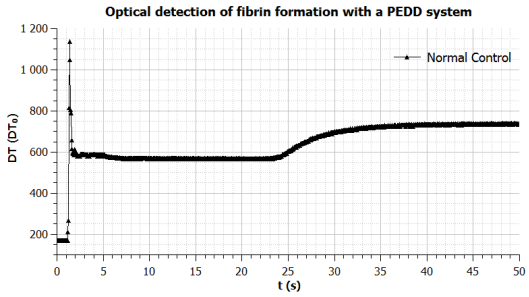

Figure 5: Optical detection of fibrin formation of a normal control plasma from *Stago* with *Neoplastine*.

A few more tests were performed to understand if the ratio between the sample and reagent (S:R) altered the results, using *Neoplastine* and a normal *Stago* control. Coagulation times and normalised ΔDT_{Coag} are shown in table 1.

S:R	1:1	1:2	1:3	1:4
$\Delta DT_{Coag_{norm}}(\%)$	19.58	15.73	15.18	8.69
t_{Coag} (s)	16.16	17.63	19.43	24.19

Table 1: Coagulation times and normalised $\Delta DT_{Coag}(\%)$ for different S:R ratios.

The results show that using more reagent for the same volume of control plasma increases the coagulation time. It also alters the signal variation observed, which gets smaller for smaller S:R ratios. The 1:1 ratio is used in further tests until otherwise mentioned.

Finally, the possibility of diluting the reagent was explored. The reagent was diluted in distilled water in the proportion $V_{Reagent} : V_{Reagent+H_2O}$. The smaller the ratio, the bigger is the dilution. The normalised ΔDT_{Coag} and coagulation times for each dilution tested are shown in table 2.

Dilution	1:1	1:2	1:5	1:10
$\Delta DT_{Coag_{norm}}(\%)$	16.26	16.30	11.31	7.29
t_{Coag} (s)	24.72	25.82	33.41	41.23

Table 2: Coagulation times for different dilutions of the reagent.

Coagulation times increased for bigger dilutions. The normalised ΔDT_{Coag} did not vary significantly between the test using the reagent directly and the 1:2 dilution. For bigger dilutions the coagulation signal variation decreases. The 1:2 dilution was used in further tests until otherwise mentioned.

4.2. Tests with *spinit*®

Meanwhile, a double-beam spectrophotometer was used to o understand if the PT assay could be performed using an emitter LED with $\lambda = 605$ nm, since this is a wavelength that has already been studied and characterised when used inside the *spinit*®. The reactions consisted of mixing $40\mu L$ of diluted reagent with 40 μL of a normal control plasma, and placing the mixture inside the detection cell. The whole process took approximately 15 $\pm$ $2s$. For wavelengths above 500 nm the transmittance variation during fibrin formation was practically the same, despite the fact that for higher wavelengths the transmittance values were higher.

The coagulation times obtained in the previous tests, performed with a normal control, were sometimes lower than $20s$. Such short times demand an almost instantaneous efficient mixing of the reagent and sample, a very fast delivery to the detection chamber, and also a fast way of finding the chamber where the reaction is taking place. These three aspects were the basis for further testing.

4.3. Mixing Structures

A first layout was made, shown in fig.6. Structures 5 and 6 were thought of in order to understand the influence of the intervening fluids' viscosities in the mixing process. The main goal was to see whether the reagent was more or less viscous than the plasma, and then, try to add the denser fluid on top of the other, to see if the deposition was, on its own, enough to obtain a homogeneous mixture. Structures 3 and 4 were based on the structure proposed by Ju-Nan Kuo and Bo-Shiun Li. All structures are $200\mu m$ deep and 0.508 mm wide.

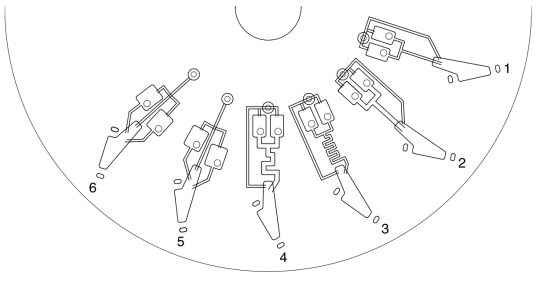

Figure 6: 1st. microfluidic disc layout.

One disc was tested with coloured water and reagent, as coloured water has a similar density to that of plasma, approximately 1025 Kg/m^3, and the mixing process was seen in real-time. Fig.7 shows the results obtained in chambers 3 to 6, after rotating the disc for $5s$ at $1000rpm$. Structures 1, 2, 5 and 6 resulted in very heterogeneous final results, with the reagent occupying the bottom of the chamber. Structures 3 and 4 resulted in more homogeneous mixtures, from which the first one is the best. This structure was chosen to perform the study of the different reagents in-house inside the *spinit*®.

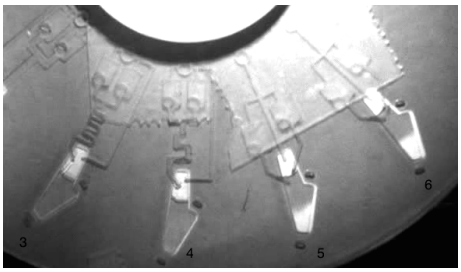

Figure 7: Results for the 1st. microfluidic disc layout using equal volumes of coloured water and Neoplastine reagent, after a $5s$ rotation at $1000rpm$.

Thromboplastins from three different brands was tested: *Stago*, *Sigma* and *Diagen*, all three of them meant for mechanical detection of clot formation. After a basic preparation of each reagent, the one from Sigma was excluded as an option, as it turned out to be very heterogeneous, with visible particles in suspension.

Both reagents from *Stago* and *Diagen* were tested with the calibrators available from each brand. The results obtained with the reagent from *Diagen* did not show a perceptible pattern. The reagent from *Stago*, on the other hand, allowed to obtain curves that showed a similar behaviour for all different calibrators. All the tests were performed at room temperature.

Despite the fact that the third structure of the first layout was the one that allowed to obtain a better mixture, this structure was still not ideal, as the mixture obtained in the detection chamber after each test was not homogeneous to the naked eye. The lack of homogeny of the final mixture might explain the imprecision values of the coagulation times obtained when mixing $4.5\mu L$ of the dilution of *Stago* reagent in purified water (1:2) with $4.5\mu L$ of calibrator plasmas.

The coefficient of variation (CV) was determined for each calibrator value, using the eq.14. N is the number of duplicates considered, and $\bar{x}$ is the average of all the results considered.

$$CV = \frac{\sqrt{\frac{\sum_{i=1}^{N}(x_i - \bar{x})^2}{N-1}}}{\bar{x}} \tag{14}$$

Duplicates were run for each calibrator, and the data was analysed in different ways, in order to understand how the coagulation times could be extracted from a curve partially similar to that shown

in fig.5. The calibration curves obtained for three different coagulation time references are shown in fig.8. Table 9 has the *CVs* obtained for each calibrator, for all three time references.

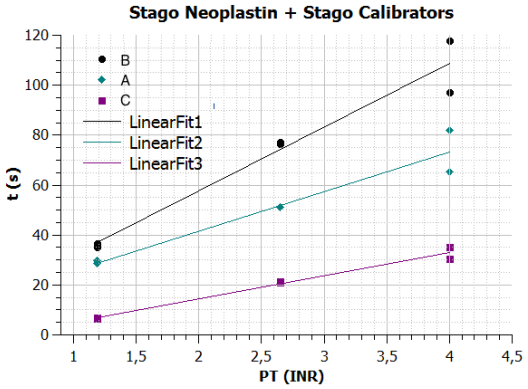

Figure 8: Calibration curves for structure 3 of the first mixing layout.

Time Reference	1.19	2.65	4.00
A	2.61	0.34	16.02
B	2.34	0.46	13.60
C	1.19	0.71	8.36

Figure 9: table
CVs for all three *Stago* calibrators, using structure 3 from the 1st mixing layout.

In order to obtain a more efficient mixing, a new layout was made, shown in fig.10. This time it consisted of slightly more complex structures, that make the reagent and sample split and collide several times before reaching the detection chamber. All the structures are $200\mu m$ deep and $0.508mm$ wide.

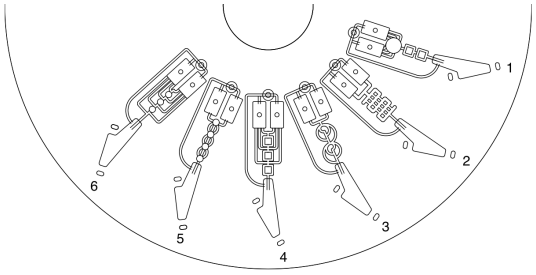

Figure 10: 2nd microfluidic disc layout.

Two different coagulation time references, A and B, were determined for each structure. Even though triplicates were made for each calibrator in each structure, several results were lost because the chamber was not detected in time. This required a revision of the centrifugation protocol used and also the settings of the *PEDD* setup. Also, no further tests were made because the number of discs available was limited. In this case, the determination of the CVs did not make sense because for most of the structures there are no replicates for time reference A, which makes it difficult to compare the results with the ones obtained with time reference B.

Some conclusions could still be made. Structures 1 and 4 were the ones that allowed to obtain coagulation times with the expected pattern, meaning that for the calibrators with higher INR values, the coagulation times obtained were also higher, for both time references considered. Structures 5 and 6 also show an expected pattern, although the imprecision between replicates was bigger than the one obtained for structures 1 and 4.

A third mixing layout was made, to understand how much the mixing quality changes when using serpentine structures with different depths, widths, number of turns, etc. The layout of the disc is shown in fig.11. Structure 6 was chosen as reference. It is $0.508\ \mu m$ wide and $200\ \mu m$ deep. Structure 2 is similar to structure 6 except in depth, which is $300\mu m$. Structures 5, 4 and 3 are all $200\ \mu m$ deep and $0.508\ \mu m$ wide. The variables that change when compared to the reference structure are the number of turns, width of the turns and shape of the turns, respectively. Finally, structure 1 has a larger width than structure 6.

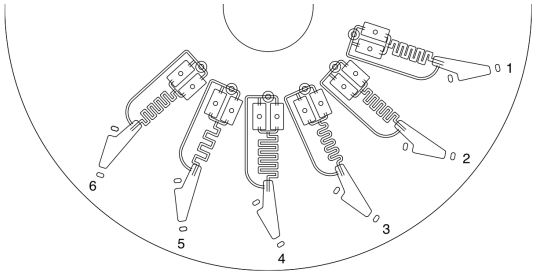

Figure 11: 3rd microfluidic mixing disc layout.

Despite the changes made to the protocol and system settings, the minimum time detected was often slightly higher than 20 s, which did not allow to obtain the coagulation times for the lower calibrator, with an $INR = 1.19$, for time reference A. Also, in other cases, the signal obtained did not show the expected behaviour. This might have to do with the reagent dilution not being completely homogeneous, or maybe the reaction was affected by the hydrophilic film.

Str.	1	2	3	4	5	6
1.19	-	-	-	-	-	-
2.65	8.34	9.23	16.94	8.29	5.76	5.82
4.00	8.75	25.65	4.96	7.28	7.04	7.07

Table 3: *CVs* for time reference A, for all *Stago* calibrators, for the 3rd layout.

Struct.	1	2	3	4	5	6
1.19	7.51	12.26	-	6.48	38.73	6.93
2.65	10.75	25.05	18.36	2.92	4.33	15.07
4.00	5.34	25.09	12.76	27.85	8.24	9.23

Table 4: *CVs* for time reference *B*, for all three *Stago* calibrators, for the 3rd layout.

All the points per reference value were considered in the determination of the *CVs*. This means that the results can not be strictly compared to each other because the number of replicates is not the same for every calibrator, allowing to make only qualitative comparisons.

The data presented in tables 3 and 4 shows that when the *CVs* of a specific structure and regarding one of the time references is more or less similar between calibrators, then the correspondent *CVs* for the other time reference varies significantly. There is no apparent reason. Also, for all the structures, except structure 2, the *CVs* are more consistent for time reference *A*, which could be considered the best way of determining the *PT*. However, it is not useful if the times for small *INR* values can not be detected. Structure 2 gave the worst results, based on the high *CVs* for all the calibrators, for both time references. The data available is not enough to evaluate which structure is the best.

One last layout was tested (fig.12), which included modifications in the mixing structures and in the detection chambers. Structure 12 was chosen as reference, with dimensions similar to the ones of the reference structure of the previous mixing layout. Only its position is different, since it is further away from the disc centre. All structures have $0.508\mu m$ channels that are $200\mu m$ deep. Structures 8 to 12 and 18 were included in order to have a link between this completely new layout and the third mixing layout. Structures 4, 14, 16 and 20 were thought of in order to make the fluid go through a channel that gets narrower and larger several times while the fluid is being pulled outwards the centre of rotation. In these structures the narrower parts are $0.508\mu m$ wide, whilst the larger ones are three times larger. Structures 2, 6 and 24 lead to fluid separation and collision in three different places.

In this test the proportion of reagent and sample used was altered, in order to use less plasma per test. $2.5\mu L$ of sample were used with $5\mu L$ of reagent.

Each calibrator was tested in triplicate, for each structure. In some tests the chamber was not detected in time to observe any of the two time references. These results were discarded. In this case all the signals detected behaved in an expected way.

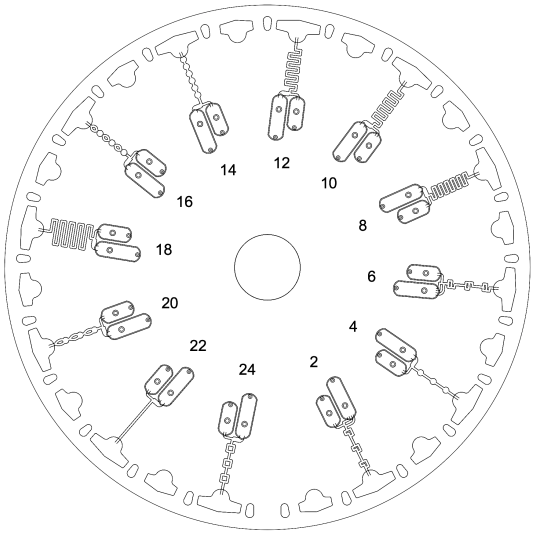

Figure 12: Fourth microfluidic mixing disc layout. All structures were milled with a milling cuter with a $0.508mm$ diameter..

The *CVs* shown in tables 4.3 and 4.3 were determined with two points for each *INR* value, for each structure. In some cases the reference time was assumed to be the first instant of detection, if it seemed to have occurred almost immediately before.

Struct.	2	4	6	8	12	14
1.28	16.41	15.94	-	-	4.59	0.14
2.65	2.56	1.73	5.32	7.46	4.42	24.00
4.00	12.97	-	8.21	1.76	7.71	10.93
Struct.	16	18	20	22	24	
1.19	8.75	5.45	7.10	6.47	5.56	
2.65	14.68	0.90	4.14	4.19	2.38	
4.00	3.43	2.18	-	8.23	2.15	

Table 5: *CVs* of the time reference *A*, for all three *Stago* calibrators, for each structure of the 4th layout.

Once again, the results obtained with each structure from every mixing layout are not enough to make a statistical study of the efficiency of each structure. This could be done if the experiment was repeated several times, so that the inter- and intra-assay imprecision could be determined and studied. It is still possible to understand which structures create a better mixing, based on the data collected, keeping in mind that future repetitions of the experiment should be done in order to confirm the results.

Using this new layout, almost all the *CVs* were

Struct.	2	4	6	8	12	14
1.28	4.92	11.71	-	-	14.65	46.73
2.65	3.67	0.17	1.25	5.09	3.64	13.64
4.00	9.60	-	4.69	1.12	8.95	11.59
Struct.	16	18	20	22	24	
1.19	1.63	4.04	11.30	0.76	2.66	
2.65	3.52	5.34	3.45	15.07	3.24	
4.00	0.95	7.20	1.78	6.93	3.56	

Table 6: *CVs* of the time reference *B*, for all three *Stago* calibrators, for each structure of the 4th layout.

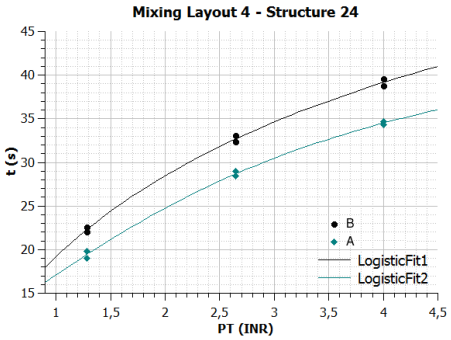

Figure 13: Calibration curves for structure 24 of the 4th mixing layout.

significantly lower than the ones obtained using the third mixing layout. Structure 14 originated the worst mixing, with *CVs* for almost all the calibrators, for both time references higher than 10%. The very low *CV* for the 1.19 *INR* calibrator using time reference *A*can be explained by the fact that both times used in its determination were considered the first detection instant, which was very similar. One might expect that a simple straight channel such as structure 22 would originate the worst mixing. However, structure 22 turned out to originate more precise replicates than structure 14, which incorporates width variations of the channel.

The mixing structure which consistently gave low *CVs* for all the calibrators, for both time references, is structure 24 (fig.13). This consistency is a good indicator of the structure mixing potential. Other structures could be considered just as good, if no extrapolation was needed, and also if different calibration curves were used.

The acceptability of the results depends on the analytical error allowable, which is 15% total error for the *PT*. However, the determination of the total error requires that real samples are tested, which is why it was not determined in this study.

5. Conclusions

The development of mixing structures that allow rapid and efficient mixing is essential in microfluidics. In the specific case of coagulation assays, this is especially important, since the coagulation process can occur within a few seconds only.

The results shown in this study show that a structure as simple as a serpentine can allow to obtain more homogeneous mixtures than more complex structures. If two similar volumes of fluids with relatively similar densities are pushed towards the outer radius almost simultaneously, through a path that offers some kind of resistance, then the fluids will be better mixed than if they were simply directly introduced in the detection chamber through a large channel. The resistance can be provoked by forcing the fluid movement to change direction, by narrowing the channels in which the fluids travel, or by inducing fluid separation and collision.

The *CVs* obtained for some of the structures were very low, within the specified analytical performance criteria. However, more replicates in different days are needed to assure the system performance. For the Prothrombin Time, the total error allowed is 15%. However, since no real samples were tested, no total errors were determined.

6. Future Work

The results obtained in this study are encouraging, especially taking into account that this particular assay is usually performed with mechanical or electrochemical detection methods.

The next step will be performing this assay with real plasma samples and then using capillary blood, provided in real time. Then, it will be the implementation of an optimised version of this system into a disc with all the microfluidic necessary to separate whole blood into blood cells and plasma, reconstitute dried reagents, and also meter the necessary volumes. Such microfluidic structures have already been developed in *biosurfit*.

A further study is needed to understand the impact of the malfunction of each coagulation factor of the extrinsic path in the overall coagulation signal obtained. This study could also help understand if t is possible to detect malfunctioning factors doing a single *PT* test using the method described in this study, instead of individual tests with different reagents, for each factor.

The results of this study are now being further developed within the scope of a new project in *biosurfit*.

Acknowledgements

I am deeply grateful for the opportunity given to me by my supervisor João Fonseca to develop this thesis at *biosurfit*. It was an amazing experience that allowed me to know and work with bright, passion-

ate people who really enjoy every minute of what they are doing, and who made me feel part of the team from the first moment.

I would also like to thank my family and friends, especially my amazing parents and brother, for all the pep talks, patience and never-ending support over the last years. Thank you all so much!

References

[1] G. D. Boon. An overview of hemostasis. *Toxicologic pathology*, 21(2):170–179, 1993.

[2] J. D. http://en.wikipedia.org/wiki/coagulation #mediaviewer/file:coagulation_full.svg.

[3] B. Dabkowski. Coagulation analysers - point of care, self monitoring. *CAP Today*, pages 12 – 22, May 2013.

[4] J. Ducrée, S. Haeberle, S. Lutz, S. Pausch, F. Von Stetten, and R. Zengerle. The centrifugal microfluidic bio-disk platform. *Journal of Micromechanics and Microengineering*, 17(7):S103, 2007.

[5] M. Faivre, P. Peltié, A. Planat-Chrétien, M.-L. Cosnier, M. Cubizolles, C. Nougier, C. Négrier, and P. Pouteau. Coagulation dynamics of a blood sample by multiple scattering analysis. *Journal of biomedical optics*, 16(5):057001–057001, 2011.

[6] R. Gorkin, M. Czugala, C. Rovira-Borras, J. Ducree, D. Diamond, and F. Benito-Lopez. A wireless paired emitter detector diode device as an optical sensor for lab-on-a-disc applications. In *Solid-State Sensors, Actuators and Microsystems Conference (TRANSDUCERS), 2011 16th International*, pages 2526–2529. IEEE, 2011.

[7] M. Grumann. Readout of diagnostic assays on a centrifugal microfluidic platform. *Universitat Freiburg im Breisgau*, 2005.

[8] C. Hancher, L. Thacker, and E. Phares. A fiber-optic retroreflective turbidimeter for continuously monitoring cell concentration during fermentation. *Biotechnology and bioengineering*, 16(4):475–484, 1974.

[9] M. Hoffman and D. M. Monroe. Coagulation 2006: a modern view of hemostasis. *Hematology/oncology clinics of North America*, 21(1):1–11, 2007.

[10] C.-C. Hong, J.-W. Choi, and C. H. Ahn. A novel in-plane passive microfluidic mixer with modified tesla structures. *Lab on a Chip*, 4(2):109–113, 2004.

[11] J. Horsti, H. Uppa, and J. A. Vilpo. Poor agreement among prothrombin time international normalized ratio methods: comparison of seven commercial reagents. *Clinical chemistry*, 51(3):553–560, 2005.

[12] N. Ichikawa, K. Hosokawa, and R. Maeda. Interface motion of capillary-driven flow in rectangular microchannel. *Journal of colloid and interface science*, 280(1):155–164, 2004.

[13] J.-N. Kuo and B.-S. Li. Lab-on-cd microfluidic platform for rapid separation and mixing of plasma from whole blood. *Biomedical microdevices*, 16(4):549–558, 2014.

[14] K.-T. Lau, S. Baldwin, E. McHugh, and D. Diamond. Paired emitter-detector light emitting diodes for the measurement of lead(ii) and cadmium(ii=. *Analytica Chimica Acta*, 569:221–226, 2006.

[15] K.-T. Lau, S. Baldwin, M. OToole, R. Shepherd, W. J. Yerazunis, S. Izuo, S. Ueyama, and D. Diamond. A low-cost optical sensing device based on paired emitter–detector light emitting diodes. *Analytica Chimica Acta*, 557(1):111–116, 2006.

[16] R. G. Macfarlane. An enzyme cascade in the blood clotting mechanism, and its function as a biological amplifier. *Nature*, (202):498 – 499, May 1964.

[17] M. Madou, J. Zoval, G. Jia, H. Kido, J. Kim, and N. Kim. Lab on a cd. *Annu. Rev. Biomed. Eng.*, 8:601–628, 2006.

[18] C. Mathers, D. M. Fat, and J. T. Boerma. *The global burden of disease: 2004 update*. World Health Organization, 2008.

[19] E. Mieczkowska, R. Koncki, and Ł. Tymecki. Hemoglobin determination with paired emitter detector diode. *Analytical and bioanalytical chemistry*, 399(9):3293–3297, 2011.

[20] J. Steigert, M. Grumann, T. Brenner, L. Riegger, J. Harter, R. Zengerle, and J. Ducrée. Fully integrated whole blood testing by real-time absorption measurement on a centrifugal platform. *Lab on a Chip*, 6(8):1040–1044, 2006.

[21] J. Steigert, M. Grumann, M. Dube, W. Streule, L. Riegger, T. Brenner, P. Koltay, K. Mittmann, R. Zengerle, and J. Ducrée. Direct hemoglobin measurement on a centrifugal microfluidic platform for point-of-care diagnostics. *Sensors and Actuators A: Physical*, 130:228–233, 2006.

[22] F. Thomaz. *spinit*® clinical chemistry assay, master thesis. *Instituto Superior Técnico*, 2014.

[23] Ł. Tymecki, M. Pokrzywnicka, and R. Koncki. Paired emitter detector diode (pedd)-based photometry–an alternative approach. *Analyst*, 133(11):1501–1504, 2008.